PAPER

Check for updates

Synthesis, biological and pharmacokinetic characterization of a novel leucine ureido derivative as a multi-target anticancer agent†

Fangyuan Shi,[a] Qifu Xu,[b] Yingjie Zhang, [ID][b] Jiangying Cao,*[c] Chunxi Liu*[a] and Anchang Liu*[a]

Previously, a novel series of leucine ureido derivatives containing the 1,2,3-triazole moiety were identified and validated as potent aminopeptidase N inhibitors with marked *in vitro* and *in vivo* antitumor potencies. Moreover, synergistic anti-proliferation effects against tumor cells were found when used in combination with 5-Fluorouracil (5-FU). Herein, a novel leucine ureido derivative (compound **3**) was synthesized by coupling cytotoxic agent 5-FU with leucine ureido derivatives containing the 1,2,3-triazole moiety *via* esterification. The biological activity evaluation showed that compound **3** exhibited more potent *in vitro* anti-proliferative, anti-metastatic, anti-angiogenic activities than the positive control bestatin. Furthermore, it was observed that compound **3** was very stable in simulated gastric fluid, while slowly cleaved in simulated intestinal fluid. *In vivo* pharmacokinetic study displayed that compound **3** was absorbed quickly after oral administration in rats and maintained *in vivo* for a long time, but exhibited poor oral bioavailability. Generally speaking, compound **3** is a promising lead for further development of more potent analogs as anticancer agents.

1. Introduction

Aminopeptidase N (APN; CD13; EC 3.4.11.2) belonging to the M1 family of the MA clan of peptidase is a Zn^{2+} dependent membrane-bound exopeptidase,[1,2] which consist of a short cytoplasmic domain, a single transmembrane part and a large extra-cellular domain.[3] As a moonlighting protein, APN presents multiple biological functions, such as enzymatic activity, antigen presentation and the receptor for some viruses.[4] It was reported that APN was associated with the tumor migration, invasion, metastasis and angiogenesis.[5–7] Moreover, APN is a functional marker of semi-dormant liver cancer cells which are responsible for chemotherapy resistance and cancer relapse.[8]

Due to the important role of APN in tumors, APN inhibitors (APNIs) had caught the attention of scientists. So far, many APN inhibitors have been reported.[9,10] Bestatin, containing an AHPA skeleton, has displayed diverse biological activities, such as anti-angiogenic, anti-metastatic, and immunomodulatory

effects.[11,12] 5-Fluorouracil (5-FU, compound **1**), a pyrimidine fluoride derivative, presents inhibitory activities against various carcinomas. However, it is limited in clinical application due to the side effects and shortcomings, such as marrow toxicity, short plasma half-life, and poor tumor selectivity.[13] Therefore, the N^1 and N^3 positions of 5-FU were usually modified with biodegradable linkers to generate prodrugs to improve the efficacy and reduce toxicity.[14,15]

In the previous work of our group, we synthesized a number of different series of APN inhibitors, of which the leucine ureido derivatives with the 1,2,3-triazole moiety (compound **2**) exhibited excellent APN inhibitory potency and promising *in vitro* and *in vivo* anti-angiogenic and anti-metastatic effects.[16,17] Notably, when combined with 5-fluorouracil (5-FU), synergistic anti-proliferation effects against several tumor cell lines were exhibited and no significant systemic toxicity was found in a mouse hepatoma H22 tumor transplant model.[16]

According to the multi-target drug design approach,[18,19] we designed a new leucine ureido derivative (compound **3**, Fig. 1) by coupling 5-FU moiety with the carboxyl group of leucine ureido derivatives containing the 1,2,3-triazole group. In detail, the ester linker was liable and could be cleaved by the esterase enzyme. Moreover, the hydroxymethyl-5-FU (compound **4**) could be converted to 5-FU *via* an extremely fast process. Therefore, the hybrid drug was supposed to release cytotoxic agent 5-FU and compound **5** by the enzyme-catalyzed metabolic reactions. In addition, compound **3** might have enhanced antitumor activity due to the aforementioned synergistic anti-

[a]*Department of Pharmacy, Qilu Hospital of Shandong University, Jinan, Shandong, 250012, China. E-mail: acleu@126.com; liuchunxi1985@163.com*

[b]*Department of Medicinal Chemistry, Key Laboratory of Chemical Biology (Ministry of Education), School of Pharmaceutical Sciences, Cheeloo College of Medicine, Shandong University, Jinan, Shandong 250012, P. R. China*

[c]*School of Pharmacy, Shandong University of Traditional Chinese Medicine, Jinan, Shandong 250355, P. R. China. E-mail: 60030103@sdutcm.edu.cn*

† Electronic supplementary information (ESI) available. See DOI: https://doi.org/10.1039/d4ra03200d
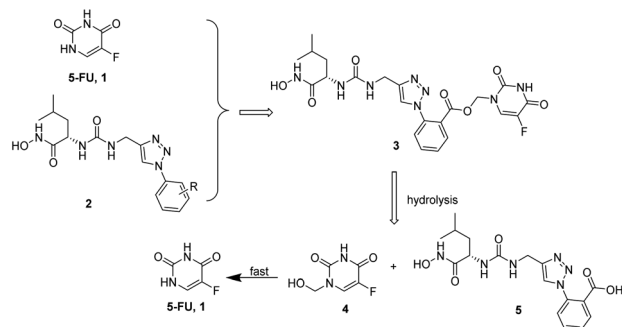
Paper

Fig. 1 Design strategy and proposed degradation pathway for the target compound.

proliferation effects of 5-FU combined with the leucine ureido derivatives against tumor cells.[16] Thereby, the *in vitro* anti-proliferative activities, stability and *in vivo* pharmacokinetic properties of compound **3** are reported in this paper.

2. Results and discussion

2.1. Chemistry

The target compound **3** is synthesized following the routes in Schemes 1 and 2. As shown in Scheme 1, compound **6** reacted with triphosgene to generate isocyanate, which was then immediately reacted with propargylamine to yield the ureido derivative **7**. Then, NH_2OK transformed the methyl ester group of **7** to hydroxamate moiety to give the key intermediate **8**.

As shown in Scheme 2, activation of the amino groups of the aromatic amine **9** with sodium nitrite in 10% hydrochloric acid and then reacted with sodium azide led to the azide derivative **10**, which was hydrolyzed with sodium hydroxide to obtain carboxyl derivative **11**. 5-Fluorouracil (**1**) was reacted with 37% oxymethylene to give the hydroxymethylated intermediate **4**, which was coupled with **11** *via* esterification of carboxyl and hydroxyl group to give intermediate **12**. Finally, the target compound **3** was generated by coupling **12** with **8** *via* click chemistry.

2.2. Enzyme inhibitory activity of the target compound against porcine APN

The target compound **3** synthesized was firstly evaluated for the inhibitory activity against porcine APN with bestatin as the positive control. The results in Table 1 showed that the APN inhibitory activity of compound **3**, with the IC_{50} value of 0.50 ± 0.2 μM, was over 8-fold more potent than the positive control bestatin (APN $IC_{50} = 4.08 \pm 0.35$ μM).
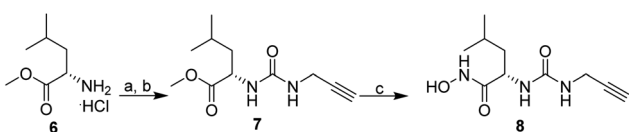
Scheme 1 Reagents and conditions: (a) triphosgene, $NaHCO_3$, DCM/H_2O, 0 °C, 1.5 h; (b) propargylamine, TEA, DCM, 25 °C, 12 h; (c) NH_2OK, MeOH, 25 °C, 0.5 h.
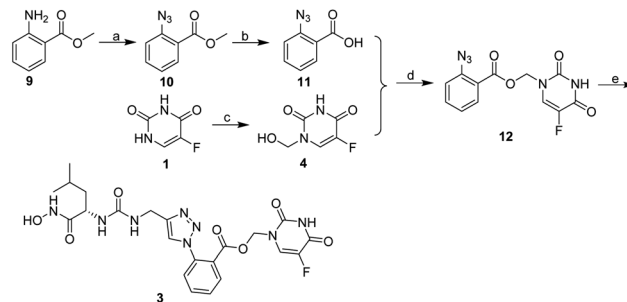
Scheme 2 Reagents and conditions: (a(i)) 10% HCl, $NaNO_2$, 0 °C, 0.5 h, (ii) NaN_3, 0 °C, 0.5 h; (b) NaOH, H_2O, MeOH, 25 °C, 3 h; (c) 37% oxymethylene, 70 °C, 2 h; (d) PyBOP, Et_3N, DCM, THF, 24 h; (e) 8, $CuSO_4 \cdot 5H_2O$, sodium ascorbate, DMSO/H_2O (4 : 1), 25 °C, 5 h.

Table 1 The IC_{50} value of the target compound against APN from porcine kidney

Compd	$IC_{50}{}^a$ (μM)
3	0.50 ± 0.29
Bestatin	4.08 ± 0.35

^{a} Assays were performed in triplicate; data are shown as mean $\pm$ SD.

2.3. *In vitro* anti-proliferative activities of the target compound against tumor cells

Compound **3** was further evaluated in the anti-proliferation assay against six tumor cell lines (MDA-MB-231, HEL, K562, HuH7, PLC/PRF/5 and HepG2). The results are listed in Table 2. Compared with other tumor cells, HEL and K562 cell lines were more sensitive to compound **3**, with the IC_{50} values of 47.18 ± 19.29 μM and 25.58 ± 12.31 μM, respectively. Moreover, compound **3** presented better anti-proliferative potencies than bestatin against HEL and K562 cell lines.

2.4. *In vitro* and *ex vivo* anti-angiogenesis assays

To evaluate the *in vitro* anti-angiogenic potency of compound **3**, the human umbilical vein endothelial cells (HUVECs) tubular structure formation assay was performed. The results in Fig. 2 showed that compound **3** could inhibit the capillary tube formation at the concentration of 5 μM. Moreover, compared with 10 μM of bestatin, 5 μM of compound **3** presented less tubular structure formed by HUVECs, indicating the better anti-angiogenesis activity.

It is well-known that the rat aortic ring model could simulate the *in vivo* angiogenesis environment better than the HUVECs tube formation model. The *ex vivo* rat thoracic aorta ring assay was used to further evaluate the anti-angiogenic activity of compound **3**. The results are shown in Fig. 3. Compared with the control group, compound **3** could prevent the micro-vessel growth at the concentration of 5 μM. Moreover, similar with the results shown in the HUVECs tubular structure formation assay, 5 μM of compound **3** demonstrated much better inhibitory potency against micro-vessel growth relative to 10 μM of bestatin.

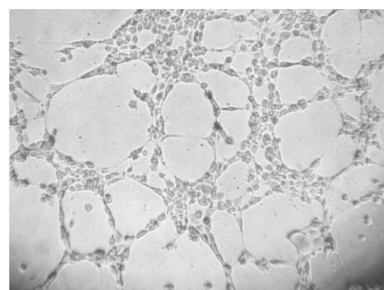**Table 2** The IC$_{50}$ values of target compound against proliferation of the tumor cell lines

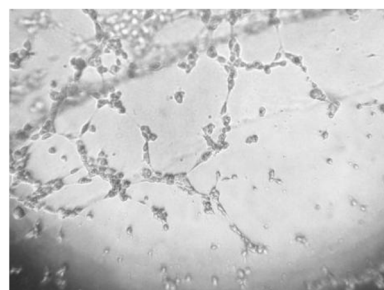| Compd	IC$_{50}$^{a} (μM)					
	MDA-MB-231	HEL	K562	HuH7	PLC/PRF/5	HEPG2
3	>100	47.18 ± 19.29	25.58 ± 12.31	>100	>100	>100
Bestatin	>100	>100	>100	>100	>100	>100

^{a} Assays were performed in triplicate; data are shown as mean ± SD.
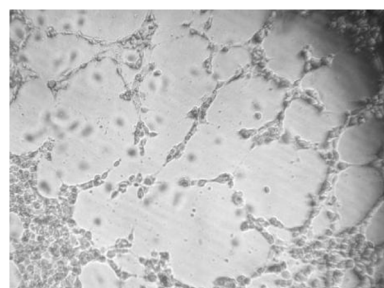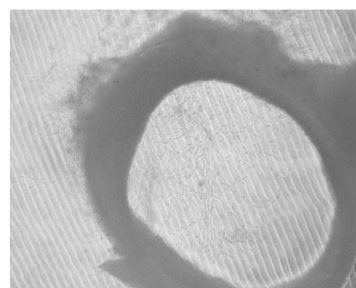

Ctrl

Bestatin (10 μM)

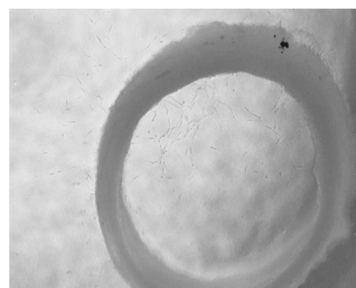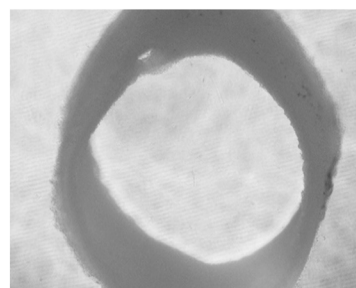Comp. **3** (5 μM)

Fig. 2 Representative images of compound **3** on the formation of HUVECs capillary tube-like structure.

Ctrl

Bestatin (10μM)

Comp. **3** (5μM)

Fig. 3 Representative images of compound **3** on the micro-vessels growth of the rat aortic ring.

2.5. Stability of the test compound *in vitro*

The stability of compound **3** in simulated gastric fluid and simulated intestinal fluid was conducted using a LC/MS/MS method. Briefly, the compound **3** was incubated at 37 °C for the appointed time. At predetermined time points, a sample of the mixture was removed, mixed, centrifuged and analyzed by LC/MS/MS. It was observed that compound **3** was very stable in simulated gastric fluid, while slowly cleaved in simulated intestinal fluid (Fig. 4). The results showed that compound **3** could release significant levels of compound **5** and 5-FU *in vitro*.

Therefore, the anti-proliferative activities of compound **3** against tumor cells might be partly due to the synergistic effect of compound **5** and 5-FU.

2.6. Metabolic stability in mouse liver microsomes (MLMs)

Metabolic stability assay of compound **3** with testosterone as the positive control, was performed in liver microsomes of mouse at the concentration of 1 μM. The metabolism of compound **3** in mouse liver microsomes was determined for
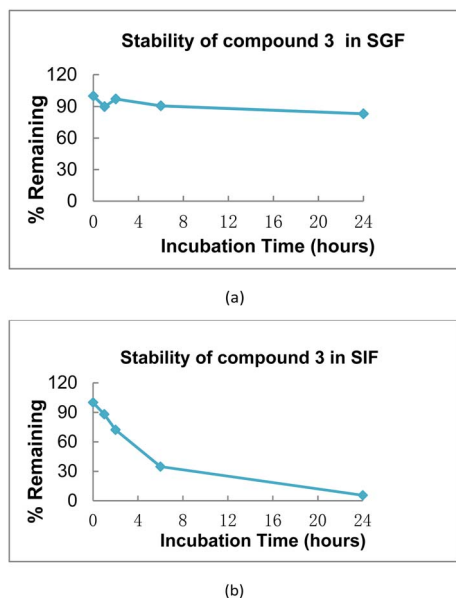
Stability of compound 3 in SGF

(a)

Stability of compound 3 in SIF

(b)

Fig. 4 (a) Stability of compound **3** in simulated gastric fluid, points were achieved after 0, 1, 2, 6, 24 h, respectively; (b) stability of compound **3** in simulated intestinal fluid, points were achieved after 0, 1, 2, 6, 24 h, respectively.

phase I oxidative reactions. The results were listed in Table 3. Compound **3** was stable in MLMs with $T_{1/2} = 94.9$ min and $CL_{int}(liver) = 57.8$ mL min^{-1} kg^{-1}. The remaining amount of compound **3** at 60 min was 69.4% in MLMs, comparing with the group with no co-factor, which indicated that NADPH was involved in the metabolism of the target compound.

2.7. *In vivo* PK studies

Given its promising results in the *in vitro* studies, the *in vivo* pharmacokinetic properties of compound **3** were assayed after a single intravenous (i.v.) or oral (p.o.) administration, respectively, which could be beneficial for the further preclinical studies.

The degradation kinetics of compound **3** *in vivo* was evaluated in Sprague Dawley rats (Table 4 and Fig. 5), and LC-MS/MS analysis was conducted to quantitatively determine the plasma concentration of compound **3** and the corresponding metabolites. As shown in Table 4, it was revealed that the mean values of the maximum plasma concentration (C_{max}) of compound **3** after i.v. and p.o. administration were $47\,400 \pm 15\,838$ ng mL^{-1} and 337 ± 158 ng mL^{-1}, respectively. The areas under the plasma concentration–time curve extrapolated to the last time

point (AUC_{0-t}) after i.v. and p.o. administration were $16\,059 \pm 6837$ ng h mL^{-1} and 484 ± 119 ng h mL^{-1}, respectively. Moreover, the plasma $T_{1/2}$ values of compound **3** were 0.867 ± 0.387 h (i.v.) and 4.44 ± 4.1 h (p.o.), respectively. The time to C_{max} (T_{max}) was 0.417 h, indicating that compound **3** was absorbed rapidly after oral administration.

As shown in Fig. 5, after administration of compound **3**, its degradation products 5-FU and compound **5** were founded almost simultaneously. Therefore, it was speculated that compound **3** was rapidly metabolized to release 5-FU and compound **5**. Although absorbed quickly in rats and maintained *in vivo* for a long time, the absolute oral bioavailability of compound **3** was determined to be 0.64%. Therefore, the attention could be focused on the optimal delivery system to increase the oral bioavailability of compound **3** and enhance the pharmacological efficacy.

3. Experimental

3.1. Chemistry: general procedures

All the commercially available materials were used without further purification otherwise noted. All reactions were monitored by thin-layer chromatography (TLC) on 0.25 mm silica gel plates (60 GF-254). The product spots were visualized by UV light, ferric chloride and iodine vapor. The purification of products was performed *via* column chromatography and recrystallization. Melting points were determined on an electrothermal melting point apparatus without correction. ^{1}H NMR and ^{13}C NMR spectra were determined on a Brucker DRX spectrometer with TMS as an internal standard. Chemical shifts were described as δ in parts per million and J in hertz. HRMS and ESI-MS were conducted by Shandong Analysis and Test Center.

3.1.1. Preparation of (*S*)-methyl 4-methyl-2-(3-(prop-2-yn-1-yl)ureido)pentanoate (7). Compound **6** (1.81 g, 10.00 mmol) was added to a mixture solution of DCM (40 mL) and saturated NaHCO$_3$ (40 mL). Then, triphosgene (0.98 g, 3.30 mmol) was added to the mixture gradually and stirred at 0 °C for 1.5 h. The organic layer was separated and dried over MgSO$_4$ for 15 min. After filtration, the filtrate was dropwise added into the solution of propargylamine (0.55 g, 10.00 mmol) and Et$_3$N (1.21 g, 12.00 mmol) in anhydrous DCM (100 mL) at 0 °C. Subsequently, the mixture was stirred at 25 °C for 12 h. DCM was concentrated under vacuum and the residue was dissolved in EtOAc (100 mL). The mixture was washed with 10% HCl (3 × 100 mL), saturated NaHCO$_3$ (3 × 100 mL) and brine (3 × 100 mL), followed by drying over MgSO$_4$ overnight. After evaporation of EtOAc, the

Table 3 Half-life and intrinsic clearance of compound **3** in mouse liver microsomes

Compd	$T_{1/2}$ (min)	CL_{int}(mic) (μL min^{-1} mg^{-1})	CL_{int}(liver) (mL min^{-1} kg^{-1})	Remaining ($T = 60$ min)	Remaining ([a]NCF = 60 min)
3	94.9	14.6	57.8	69.4%	80.1%
Testosterone	5.5	252.1	998.5	0.2	91.0%

[a] NCF: abbreviation of no co-factor.

Table 4 The pharmacokinetic parameters of compound **3** after oral or intravenous administration in rats ($n = 3$)

PK parameters	Dosed (mg kg^{-1})	C_{max} (ng mL^{-1})	T_{max} (h)	AUC$_{0-t}$ (ng h mL^{-1})	AUC$_{0-\infty}$ (ng h mL^{-1})	CL (mL h^{-1} kg^{-1})	$T_{1/2}$ (h)	F (%)
i.v.	10	$47\,400 \pm 15\,838$	0.0833 ± 0	$16\,059 \pm 6837$	$16\,067 \pm 6840$	737 ± 407	0.867 ± 0.387	NA
p.o.	50	337 ± 158	0.417 ± 0.144	484 ± 119	510 ± 99.3	NA	4.44 ± 4.1	0.64

obtained crude product was further purified by recrystallization from ethyl acetate/petroleum ether to give compound **7** as a white solid (1.87 g, yield: 83%), mp: 102.9–104.2 °C. ^{1}H NMR (300 MHz, DMSO-d_6): δ 6.37 (d, $J = 8.4$ Hz, 1H), 6.25 (t, $J = 5.7$ Hz, 1H), 4.17 (q, $J = 8.4$ Hz, 1H), 3.78 (dd, $J = 5.7$ Hz, $J = 2.4$ Hz, 2H), 3.61 (s, 3H), 3.05 (t, $J = 2.4$ Hz, 1H), 1.68–1.54 (m, 1H), 1.47–1.42 (m, 2H), 0.89–0.84 (m, 6H); ESI-MS m/z 227.4 [M + H]$^+$.

3.1.2. Preparation of (S)-N-hydroxy-4-methyl-2-(3-(prop-2-yn-1-yl)ureido)pentanamide (8). Potassium hydroxide (28.50 g, 508.93 mmol) was dissolved in anhydrous methanol (70 mL) under an ice-bath. Then the above solution was added dropwise to hydroxylamine hydrochloride (23.00 g, 330.94 mmol) in the anhydrous methanol solution (120 mL) at 0 °C. The mixture was stirred at 0 °C for 40 min and the precipitate was filtered out to give a fresh methanol solution of potassium hydroxylamine. Compound **7** (2.26 g, 10 mmol) was dissolved in the solution above (20 mL) at 25 °C, followed by stirring at 25 °C for 0.5 h. The methanol was evaporated and the residue was dissolved in water. The excess base was neutralized with 10% HCl. Then, the formed oil was extracted by EtOAc (3 × 100 mL). The organic layer was washed with saturated NaHCO$_3$ (3 × 100 mL) and brine (3 × 100 mL), and dried over MgSO$_4$. EtOAc was evaporated under vacuum, and the residue was added into DCM. The mixture was placed into refrigerator overnight. The white precipitate was formed and filtered off to give 1.20 g of compound **8**. Yield: 53%, mp: 124.5–126.2 °C. ^{1}H NMR (600 MHz, DMSO-d_6): δ 10.68 (s, 1H), 8.80 (s, 1H), 6.24 (t, $J = 5.7$ Hz, 1H), 6.16 (d, $J = 8.4$ Hz, 1H), 4.05 (q, $J = 8.4$ Hz, 1H), 3.78 (dd, $J = 5.7$ Hz, $J = 2.4$ Hz, 2H), 3.05 (t, $J = 2.4$ Hz, 1H), 1.54–1.50 (m, 1H), 1.34–1.32 (m, 2H), 0.89–0.84 (m, 6H); ESI-MS m/z 226.3 [M–H]$^-$.

3.1.3. Preparation of methyl 2-azidobenzoate (10). Compound **9** (12.08 g, 80.00 mmol) was dissolved in the 10% HCl (400 mL), and then the solution of NaNO$_2$ (5.91 g, 85.60 mmol) in H$_2$O (50 mL) was added, the mixture was stirred at 0 °C for 0.5 h. Then, the solution of NaN$_3$ (5.72 g, 88.00 mmol) in H$_2$O (50 mL) was dropwise added into the above mixture. After stirring at 0 °C for 0.5 h, the aqueous layer was extracted by EtOAc (3 × 150 mL). The organic layer was dried over MgSO$_4$ overnight. After filtration, EtOAc was evaporated to give the crude product, which was further purified by column chromatography (the fluent phase: petroleum ether) to give compound **10** as yellow oil (12.32 g, yield 87%). ^{1}H NMR (400 MHz, DMSO-d_6): δ 7.77 (d, $J = 8.0$ Hz, 1H), 7.62 (t, $J = 8.0$ Hz, 1H), 7.38 (d, $J = 8.0$ Hz, 1H), 7.27 (t, $J = 8.0$ Hz, 1H), 3.83 (s, 3H).

3.1.4. Preparation of 2-azidobenzoic acid (11). To the solution of compound **10** (8.85 g, 50.00 mmol) in the MeOH (60 mL), the 1 N NaOH aqueous solution (60 mL) was added. After stirring at 25 °C for 3 h, 10% HCl was added to adjust pH to 6. The formed precipitate was filtered off and dried under vacuum to give compound **11** as a white solid (7.99 g, yeild: 98%). mp: 140.5–141.4 °C. ^{1}H NMR (400 MHz, DMSO-d_6): δ 13.17 (s, 1H), 7.78 (d, $J = 8.0$ Hz, 1H), 7.60 (t, $J = 8.0$ Hz, 1H), 7.36 (d, $J = 8.0$ Hz, 1H), 7.27 (t, $J = 8.0$ Hz, 1H).

3.1.5. Preparation of 5-fluoro-1-(hydroxymethyl)pyrimidine-2,4(1H,3H)-dione (4). Compound **1** (2.20 g, 16.90 mmol) was dissolved in 37% oxymethylene solution (3.01 g, 37.1 mmol) and the mixture was stirred at 70 °C for 2 h. The solvent was evaporated and the residue was dried under vacuum to give compound **4** as colorless oil. The crude product was used in the next reaction without further purification.

3.1.6. Preparation of (5-fluoro-2,4-dioxo-3,4-dihydropyrimidin-1(2H)-yl)methyl 2-azidobenzoate (12). PyBOP (11.23 g, 21.60 mmol) and Et$_3$N (2.18 g, 21.60 mmol) was added to a solution of compounds **11** (2.93 g, 17.98 mmol) and **4** (2.88 g, 18.00 mmol) in anhydrous DCM (20 mL) and anhydrous THF (20 mL). After stirring at 25 °C for 24 h, the solvent was evaporated and the residue was dissolved in EtOAc (50 mL) and H$_2$O (50 mL). The formed precipitate was filtered out. The organic layer was separated and washed with brine. After dried over MgSO$_4$ overnight, EtOAc was evaporated to give the crude product, which was further purified by column chromatography (DCM/MeOH/THF = 100 : 2 : 40) to give compound **12** as a white solid (2.25 g, yield: 41%). mp: 168.4–169.8 °C. ^{1}H NMR (400 MHz, DMSO-d_6): δ 12.03 (s, 1H), 8.26 (d, $J = 6.5$ Hz, 1H), 7.82 (d, $J = 7.8$ Hz, 1H), 7.68 (t, $J = 7.8$ Hz, 1H), 7.44 (d, $J = 8.1$ Hz, 1H), 7.31 (t, $J = 7.8$ Hz, 1H), 5.80 (s, 2H).

3.1.7. Preparation of (5-fluoro-2,4-dioxo-3,4-dihydropyrimidin-1(2H)-yl)methyl (S)-2-(4-((3-(1-(hydroxyamino)-4-methyl-1-oxopentan-2-yl)ureido)methyl)-1H-1,2,3-triazol-1-yl)benzoate (3). Compounds **8** (0.53 g, 2.33 mmol) and **12** (0.78 g, 2.60 mmol) were dissolved in DMSO (16 mL), followed by the addition of sodium ascorbate (68.3 mg, 0.35 mmol) in H$_2$O (2 mL) and CuSO$_4$·5H$_2$O (30 mg, 0.12 mmol) in H$_2$O (2 mL). After stirring at 25 °C for 5 h, the mixture was poured into water (100 mL). Then, the mixture was extracted by EtOAc (3 × 100 mL). The organic layer was washed with brine (3 × 100 mL) and dried over MgSO$_4$. EtOAc was evaporated and the residue was purified by column chromatography (DCM/MeOH = 100 : 10) to give compound **3** as a white solid (0.31 g, yield: 25%). mp: 124.3–125.8 °C. ^{1}H NMR (400 MHz, DMSO-d_6): δ 11.97 (s, 1H), 10.68 (s, 1H), 8.80 (s, 1H), 8.31 (s, 1H), 8.00–7.95 (m, 2H), 7.83 (t, $J = 7.7$ Hz, 1H), 7.72 (t, $J = 7.7$ Hz, 1H), 7.65 (d, $J = 7.7$ Hz, 1H), 6.44 (t, $J = 5.7$ Hz, 1H), 6.21 (d, $J = 8.8$ Hz, 1H), 5.63 (s, 2H), 4.35–4.24 (m, 2H), 4.11–4.05 (m, 1H), 1.58–1.50 (m, 1H), 1.35 (t, $J = 7.2$ Hz,
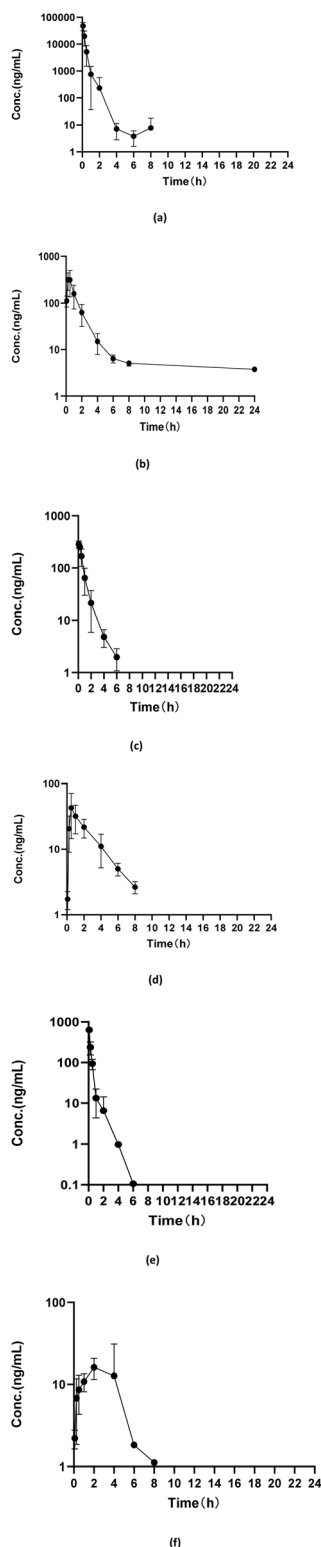
Fig. 5 (a) Concentration–time curve of compound **3** after i.v. administration in rats; (b) concentration–time curve of compound **3** after p.o. administration in rats; (c) concentration–time curve of compound **5** after i.v. administration in rats; (d) concentration–time curve of compound **5** after p.o. administration in rats; (e) concentration–time curve of compound 5-FU after i.v. administration in rats; (f) concentration–time curve of compound 5-FU after p.o. administration in rats.

2H), 0.89–0.85 (m, 6H); ^{13}C NMR (100 MHz, DMSO-d_6): δ 169.9, 165.1, 157.7, 149.5, 146.7, 141.1, 138.8, 135.7, 133.9, 131.2, 130.3, 129.7, 129.4, 126.5, 124.1, 71.3, 49.6, 42.8, 35.2, 24.6, 23.2, 22.6. Retention time: 36.03 min, eluted with MeOH/water (0.1% formic acid), purity: 97.16%.

3.2. Biological evaluation

3.2.1. APN inhibition assay. IC_{50} values of tested compounds against APN were evaluated using L-Leu-p-nitro-anilide (Sigma-Aldrich, St. Louis, MO, USA) as substrate and microsomal APN from porcine kidney microsomes (Enzo Life Sciences, Farmingdale, NY, USA) as enzyme. The substrate was dissolved in DMSO for the concentration of 16 mmol L^{-1} and the enzyme was dissolved in 50 mM PBS (pH = 7.2) to a concentration of 0.15 IU L^{-1}. The tested compounds were dissolved in DMSO for the concentration of 100 mmol L^{-1} as stock solutions, which were further diluted to the concentrations of 250 μmol L^{-1}, 62.5 μmol L^{-1}, 15.63 μmol L^{-1}, 3.91 μmol L^{-1}, 0.98 μmol L^{-1}, and 0.24 μmol L^{-1} using PBS buffer, respectively. Briefly, compounds (40 μL) were added into 96-well plates, followed by the addition of PBS (145 μL). Then, substrate (5 μL) and enzyme (10 μL) were added into the above solution in sequence. The mixture was incubated at 37 °C for 30 min. The absorbance values were measured at 405 nm with a plate reader (Varioskan, Thermo Fisher Scientific, Waltham, MA, USA).

3.2.2. Anti-proliferation assay. Anti-proliferative activities of compounds against tumor cells were evaluated by the MTT [(3-[4,5-dimethyl-2-thiazolyl]-2,5-diphenyl-2H-tetrazolium bromide)] method. Before the experiment, the tumor cells were taken out of the liquid nitrogen tank and resuscitated in a 40 °C water bath for 1 minute. Firstly, the resuscitated tumor cells were cultivated in RPMI 1640 medium with 10% FBS at 37 °C in 5% CO$_2$ humidified incubator. The MTT test was conducted when the tumor cells were in the logarithmic growth phase. Cells suspended in culture medium (100 μL) were inoculated in 96-well plates with the density of 10 000–12000 cells per well. After incubation for 4 h, compound sample (100 μL) which were previously diluted to the working concentrations (0.16/0.8/4/20/100 μmol L^{-1}) with complete medium were added to the tested 96-well plates and incubated for a further 48 h. Subsequently, MTT (20 μL, 5 mg mL^{-1}) solution was added into the test well, followed by the incubation for another 4 h. The plates were centrifuged at 800 rpm for 3 min. The supernatant was poured off and DMSO (200 μL) was added to dissolve the formed formazan. Finally, the mixture was shaken for 15 min and the absorbance values were measured using a plate reader at 570 nm (Varioskan, Thermo Fisher Scientific, Waltham, MA, USA).

3.2.3. HUVEC tubular structure formation assay. Matrigel (50 μL; BD biosciences) was added into test well of 96-well plates and then allowed to polymerize for 0.5 h at 37 °C. HUVECs were suspended in M199 medium at a density of 4×10^5 cells per mL. 50 μL of cell suspension was added into the well pre-coated with Matrigel, followed by the addition of 50 μL of compounds dissolved in M199 medium at the specified concentrations. The mixture was further incubated at 37 °C in 5% CO$_2$ for 4 h. The

tubular structures formed by HUVECs were observed under an inverted microscope and photographed at 100× magnification.

3.2.4. Rat aortic ring assay. The thoracic aortas were separated from 8 to 10 week-old male Sprague Dawley rats. After careful removal of fibroadipose tissues, the aortas were cut into 1 mm-long cross-section. The test wells of the 96-well plates were pre-coated with Matrigel (100 μL; BD bioscience) at 37 °C for 0.5 h, followed by the addition of the aortas fragments and 100 μL of Matrigel, successively. The mixture was incubated at 37 °C and 5% CO_2 for 0.5 h until the Matrigel solidified. Compounds dissolved in M199 culture medium at the test concentrations were added into the above wells, followed by the incubation at 37 °C in 5% CO_2 for 9 days. The formed microvessels were visualized by inverted microscope at 100× magnification. The M199 culture medium containing compounds was changed every three days.

3.2.5. Stability of the test compound *in vitro*. Simulated gastric fluid was prepared as follows. Dissolved 0.04 g NaCl and 0.064 g pepsin in 0.14 mL HCl and added sufficient H_2O to make the total volume of 20 mL. The pH value of the test solution was determined as 1.20 ± 0.05 by pH meter.

Simulated intestinal fluid was prepared as follows. Dissolved 0.136 g KH_2PO_4 and 0.2 g pancreatin and added sufficient H_2O to make the total volume of 20 mL. The pH value of the test solution was adjusted to 6.8 ± 0.05.

To the stock solution of compound **3** was added simulated gastric fluid and simulated intestinal fluid, of which the final test concentration was 2 μM. The mixture was incubated at 37 °C and 600 rpm for the appointed time. After incubation of 60 min, 120 min, 360 min and 1440 min, respectively, to the test samples were added 400 μL of cold acetonitrile containing 200 ng per mL tolbutamide and labetalol (internal standard) immediately. Then, 200 μL of suspension was separated and mixed with 400 μL of cold acetonitrile containing 200 ng per mL tolbutamide and labetalol again. Subsequently, samples were subjected to centrifuge at 4000 rpm, 4 °C for 20 min. 200 μL of supernatant was used for the LC/MS/MS analysis to determine the remaining amount of test compound based on peak area ratio of analyte/IS. LC/MS/MS analysis was using a ACQUITY UPLC BEH C18 column (1.7 μm 2.1 × 50 mm). Compounds were eluted with water (containing 0.1% formic acid)/acetonitrile (containing 0.1% formic acid) over 60 min. The absorbance was measured at 282 nm, the flow rate was 0.5 mL min^{-1} and the quantity of injection was 20 μL.

3.2.6. Metabolic stability in mouse liver microsomes (MLMs). CD-1 mouse (Lot#: 2010017) liver microsomes obtained from Xenotech were used to determine the metabolic stability of compound **3**. Firstly, NADPH (final concentration = 1 mM) (Lot#: 00616) and MLMs were individually added to potassium phosphate buffer (100 mM) and incubated at 37 °C for 10 min. Subsequently, compound **3** and the positive control testosterone were prepared with 5 μL DMSO and 495 μL acetonitrile (ACN), and then spiked into the reaction mixture above to achieve a final concentration of 1 μM, respectively. Samples were separated from the reaction mixture at different times (5 min, 15 min, 30 min, 45 min, and 60 min), and the reaction was terminated using cold acetonitrile (ACN, 4 °C) containing 200 ng mL^{-1} of tolbutamide and 200 ng mL^{-1} of labetalol as internal standards (IS). Each

bioanalysis plate was sealed and shaken for 10 minutes prior to LC-MS/MS analysis. The equation of first order kinetics was used to calculate $T_{1/2}$ and CL_{int}(mic) (μL min^{-1} mg^{-1}).

3.2.7. *In vivo* PK studies. The pharmacokinetic parameters of compound **3** were evaluated in male Sprague Dawley rats ($N = 3$) after an intravenous or oral administration. The rats weighing 180–220 g were purchased from Beijing Vital River Laboratory Animal Technology Co., Ltd (SCXK-2021-0011). All protocols involving animals were approved by the XBL-China Institutional Animal Care and Use Committee (IACUC no. 2022-0314). In order to adjust to the environment, the rats were supplied with water and a commercial rodent diet in a controlled room with relative humidity at 40–70% and temperature at 20–26 °C for one week prior to the study. However, the rats were fasted for 12 h before the experiment. Compound **3** was administrated intravenously at a dose of 10 mg kg^{-1} or orally at a dose of 50 mg kg^{-1}, respectively. Samples were collected at several time points up to 24 h following dose administration. Following intravenous infusion administration, blood samples were collected from the jugular vein cannula at predose as well as at 0.083 h, 0.25 h, 0.5 h, 1 h, 2 h, 4 h, 6 h, 8 h and 24 h postdose of compound **3**. Moreover, following oral dosing, 0.25 mL of blood samples were collected at predose as well as at 0.25 h, 0.5 h, 1 h, 2 h, 4 h, 6 h, 8 h and 24 h postdose of compound **3**. Rat plasma samples were separated from the blood samples by centrifugation at 6000 rpm for 3 min and stored in the freezer at −20 °C before analysis. Non-compartmental PK parameters such as area under the curve (AUC) and $T_{1/2}$ were calculated using WinNonlin 8.2. The absolute oral bioavailability of compound **3** in rats was calculated by the AUC(0–∞) ratio obtained following oral and i.v. administration.

$$F\,(\%) = (dose_{iv} \times AUC_{oral(0-\infty)})/(dose_{oral} \times AUC_{iv(0-\infty)}) \times 100\%$$

4. Conclusions

In summary, according to the previous series of leucine ureido derivatives containing the 1,2,3-triazole moiety as APN inhibitors, we designed and synthesized the conjugated compound **3** following the multi-target drug design approach. Compound **3** exhibited more potent anti-proliferative activities against two human leukemic cell lines and anti-angiogenesis activity compared with the positive control bestatin. Furthermore, the preliminary stability of compound **3** revealed that the hybrid could release significant level of compound **5** and 5-FU *in vitro*, while NADPH was involved in the metabolism. Moreover, *in vivo* PK studies revealed that compound **3** was absorbed rapidly after oral administration, but the absolute oral bioavailability was approximately 0.64% in rats. Therefore, further attention can be focused on increasing the oral bioavailability and enhancing the pharmacological efficacy.

Data availability

The data supporting this article have been included as part of the ESI.†

Author contributions

Conflicts of interest

There are no conflicts to declare.

Acknowledgements

Notes and references

1 N. D. Rawlings and A. J. Barrett, MEROPS: the peptidase database, *Nucleic Acids Res.*, 1999, **27**(1), 325–331.

2 C. Antczak, I. De Meester and B. Bauvois, Ectopeptidases in pathophysiology, *Bioessays*, 2001, **23**(3), 251–260.

3 Y. Luan and W. Xu, The structure and main functions of aminopeptidase N, *Curr. Med. Chem.*, 2007, **14**(6), 639–647.

4 P. Mina-Osorio, The moonlighting enzyme CD13: old and new functions to target, *Trends Mol. Med.*, 2008, **14**(8), 361–371.

5 T. Tokuhara, N. Hattori, H. Ishida, T. Hirai, M. Higashiyama, K. Kodama and M. Miyake, Clinical significance of aminopeptidase N in non-small cell lung cancer, *Clin. Cancer Res.*, 2006, **12**(13), 3971–3978.

6 Y. Aozuka, K. Koizumi, Y. Saitoh, Y. Ueda, H. Sakurai and I. Saiki, Anti-tumor angiogenesis effect of aminopeptidase inhibitor bestatin against B16-BL6 melanoma cells orthotopically implanted into syngeneic mice, *Cancer Lett.*, 2004, **216**(1), 35–42.

7 L. Guzman-Rojas, R. Rangel, A. Salameh, J. K. Edwards, E. Dondossola, Y. G. Kim, A. Saghatelian, R. J. Giordano, M. G. Kolonin, F. I. Staquicini, *et al.*, Cooperative effects of aminopeptidase N (CD13) expressed by nonmalignant and cancer cells within the tumor microenvironment, *Proc. Natl. Acad. Sci. U. S. A.*, 2012, **109**(5), 1637–1642.

8 N. Haraguchi, H. Ishii, K. Mimori, F. Tanaka, M. Ohkuma, H. M. Kim, H. Akita, D. Takiuchi, H. Hatano, H. Nagano, *et al.*, CD13 is a therapeutic target in human liver cancer stem cells, *J. Clin. Invest.*, 2010, **120**(9), 3326–3339.

9 A. Mucha, M. Drag, J. P. Dalton and P. Kafarski, Metallo-aminopeptidase inhibitors, *Biochimie*, 2010, **92**(11), 1509–1529.

10 S. A. Amin, N. Adhikari and T. Jha, Design of Aminopeptidase N Inhibitors as Anti-cancer Agents, *J. Med. Chem.*, 2018, **61**(15), 6468–6490.

11 Y. Mishima, Y. Terui, N. Sugimura, Y. Matsumoto-Mishima, A. Rokudai, R. Kuniyoshi and K. Hatake, Continuous treatment of bestatin induces anti-angiogenic property in endothelial cells, *Cancer Sci.*, 2007, **98**(3), 364–372.

12 M. Lis, M. Szczypka, A. Suszko and B. Obminska-Mrukowicz, Influence of bestatin, an inhibitor of aminopeptidases, on T and B lymphocyte subsets in mice, *Pol. J. Vet. Sci.*, 2011, **14**(3), 393–403.

13 Z. Y. Tian, G. J. Du, S. Q. Xie, J. Zhao, W. Y. Gao and C. J. Wang, Synthesis and bioevaluation of 5-fluorouracil derivatives, *Molecules*, 2007, **12**(11), 2450–2457.

14 X. Pan, C. Wang, F. Wang, P. Li, Z. Hu, Y. Shan and J. Zhang, Development of 5-Fluorouracil derivatives as anticancer agents, *Curr. Med. Chem.*, 2011, **18**(29), 4538–4556.

15 N. Shimma, I. Umeda, M. Arasaki, C. Murasaki, K. Masubuchi, Y. Kohchi, M. Miwa, M. Ura, N. Sawada, H. Tahara, *et al.*, The design and synthesis of a new tumor-selective fluoropyrimidine carbamate, capecitabine, *Bioorg. Med. Chem.*, 2000, **8**(7), 1697–1706.

16 J. Cao, J. Zang, X. Kong, C. Zhao, T. Chen, Y. Ran, H. Dong, W. Xu and Y. Zhang, Leucine ureido derivatives as aminopeptidase N inhibitors using click chemistry. Part II, *Bioorg. Med. Chem.*, 2019, **27**(6), 978–990.

17 J. Cao, C. Ma, J. Zang, S. Gao, Q. Gao, X. Kong, Y. Yan, X. Liang, Q. Ding, C. Zhao, *et al.*, Novel leucine ureido derivatives as aminopeptidase N inhibitors using click chemistry, *Bioorg. Med. Chem.*, 2018, **26**(12), 3145–3157.

18 Z. Chen, L. Han, M. Xu, Y. Xu and X. Qian, Rationally designed multitarget anticancer agents, *Curr. Med. Chem.*, 2013, **20**(13), 1694–1714.

19 L. M. Espinoza-Fonseca, The benefits of the multi-target approach in drug design and discovery, *Bioorg. Med. Chem.*, 2006, **14**(4), 896–897.